A small nonhuman primate model for filovirus-induced disease

Ricardo Carrion Jr.[a,b,*], **Youngtae Ro**[a,c], **Kareema Hoosien**[a], **Anysha Ticer**[a], **Kathy Brasky**[b], **Melissa de la Garza**[b], **Keith Mansfield**[d], and **Jean L. Patterson**[a]

[a]Department of Virology and Immunology, Texas Biomedical Research Institute, 7620 NW Loop 410, San Antonio, TX 78227 USA

[b]Southwest National Primate Research Center, Texas Biomedical Research Institute, 7620 NW Loop 410, San Antonio, TX 78227 USA

[c]Laboratory of Biochemistry, Graduate School of Medicine, Konkuk University, Chungju 380-701, Korea

[d]New England Primate Research Center, Harvard Medical School One Pine Hill Drive, Southborough, MA 01772, USA

Abstract

Ebolavirus and Marburgvirus are members of the filovirus family and induce a fatal hemorrhagic disease in humans and nonhuman primates with 90% case fatality. To develop a small nonhuman primate model for filovirus disease, common marmosets (*Callithrix jacchus*) were intramuscularly inoculated with wild type *Marburgvirus Musoke* or *Ebolavirus Zaire*. The infection resulted in a systemic fatal disease with clinical and morphological features closely resembling human infection. Animals experienced weight loss, fever, high virus titers in tissue, thrombocytopenia, neutrophilia, high liver transaminases and phosphatases and disseminated intravascular coagulation. Evidence of a severe disseminated viral infection characterized principally by multifocal to coalescing hepatic necrosis was seen in EBOV animals. MARV-infected animals displayed only moderate fibrin deposition in the spleen. Lymphoid necrosis and lymphocytic depletion observed in spleen. These findings provide support for the use of the common marmoset as a small nonhuman primate model for filovirus induced hemorrhagic fever.

Keywords

Introduction

Ebolavirus (EBOZ) and *Marburgvirus (MARV)*, members of the filoviridae family, are causative agents of hemorrhagic fever. Filovirus-induced disease begins with flu-like symptoms and progresses rapidly to the final stages of viral hemorrhagic fever infection, which are characterized by fever, hemorrhage, and hypotensive shock (Groseth et al., 2007;

*Corresponding author: Department of Virology and Immunology, Texas Biomedical Research Institute, P.O. Box 760549, San Antonio, TX 78245-0549 USA, Tel: (210) 258-9479, Fax: (210) 670-3329, carrion@TxBiomed.org.

Zampieri et al., 2007). Infection is fatal in up to 90% as in the case of Zaire Ebolavirus or Marburg Angola. The increased frequency of filovirus outbreaks in central and western Africa and the potential use of such agents as biological weapons underscore the need to understand pathogenesis of these viruses and to develop effective intervention strategies (Groseth et al., 2007; Peterson et al., 2004a; Peterson et al., 2004b).

Nonhuman primates (NHPs) are the preferred animal model for human filovirus infection because infection with *EBOZ* and *MARV* isolated from humans results in fatal hemorrhagic disease. Numerous species of NHPs have been used, including baboons, African green monkey, rhesus and cynomolgus macaques, to study filovirus pathogenesis because the pathology of infected NHPs is similar to that seen in humans (Bente et al., 2009; Geisbert et al., 2003b). The sporadic nature of disease outbreaks and the ethical issues associated with conducting a human vaccine trial make such a study difficult to execute. Early-stage development of vaccines has historically occurred in mouse and guinea pig models of filovirus disease, but these models use adapted viruses obtained through sequential passage in the rodent species because the wild-type virus does not cause uniform lethality (Bray et al., 1999; Connolly et al., 1999). The disease observed in rodents does not reproduce the extensive disseminated intravascular coagulation seen in human filovirus disease. Besides the requirement for an adapted virus, there are reports that the rodent models are not necessarily predictive of efficacy in NHPs (Feldmann et al., 2003; Geisbert et al., 2002; Jahrling et al., 1996). NHPs are relevant models to study infectious disease as their immune system is similar to humans and they are good predictors of efficacy in vaccine development and other intervention strategies. Licensure of a filovirus vaccine will require testing in a NHP species. The macaque model is the most frequently used model in filovirus efficacy studies involving vaccines or therapies [5]. Given the drawbacks of rodent models of filovirus disease, there is a critical need for development of a small animal model that develops disease consistent with human infection using wild-type virus.

The common marmoset (*Callithrix jacchus*) is an anthropoid primate weighing between 320 and 450 grams that is used extensively in biomedical research and provides an attractive alternative to other NHPs (Mansfield, 2003). This small-bodied primate is especially valuable in maximum containment research, where space is generally at a premium. Additionally, reagents are available to characterize immunological response to vaccines. Marmosets have been used to study a number of viral diseases including hemorrhagic fever viruses such as Lassa and Junin viruses, as well as Eastern Equine Encephalitis virus, SARS-CoV, and hepatitis GB virus B, as well as other human syndromes (Adams et al., 2008; Avila et al., 1985; Bright et al., 2004; Carrion et al., 2007a; Greenough et al., 2005; Jacob et al., 2004; Lukashevich et al., 2008; Mansfield, 2003; Weatherford et al., 2009; Weissenbacher et al., 1982). Marmoset models of Lassa hemorrhagic fever and Argentine Hemorrhagic fever have been used to validate countermeasures against the HFVs (Avila et al., 1987; Carrion et al., 2007b; Samoilovich et al., 1984; Weissenbacher et al., 1986a; Weissenbacher et al., 1986b).

Here we report that a single intramuscular injection of a common marmoset with as little as 10 plaque forming units (PFU) of either MARV or EBOV resulted in fatal hemorrhagic disease. The experimental filovirus infections induced a systemic disease with histological features similar to human infection, most notably hepatocellular necrosis and extensive fibrin deposition. The availability of a marmoset model for filovirus induced disease is especially attractive since it provides a small animal model for preclinical trials that is susceptible to viruses isolated from humans without adaptation.

RESULTS

Clinical observations

All animals appeared normal until 3 days post-infection (DPI) when, weight loss and anorexia was observed. Animals infected with 1000 PFU EBOV were also febrile (>103°F) at this time point. Animals infected with 10 PFU of EBOV developed a fever 4 DPI. Similarly, MARV infected animals developed a fever at day 5 and 6 for the high dose and low dose, respectively. After the onset of fever, the behavior of animals changed: they became depressed, had reduced stool production, and weight loss (5-7% from baseline). Just before death, febrile response resolved and some animals became hypothermic. Marmosets infected with Ebola virus succumbed to disease at four to five days DPI while MARV infected animals succumbed to disease at six to eight DPI.

Complete blood counts and biochemical analyses (Table 1) were performed on blood collected from marmosets. Beginning at 4 DPI, blood contained elevated levels of serum alanine aminotransferases (ALT), a marker of hepatocellular necrosis, which continued to increase until the animal was euthanized. GGT (gamma-glutamyltransferase) and ALP (alkaline phosphatase), measured to evaluate excretory liver functions, were elevated >30-fold above baseline. Further evidence of hepatic involvement was noted in MARV animals as a significant increase in total bilirubin (TBIL) observed just prior to death (>3 mg/DL). Hematological data showed a reduction in numbers of platelet in all animals over the course of infection with development of leukocytosis (Fig. 1). All animals experienced an increase in neutrophils and concomitant decrease in lymphocytes beginning at 2 DPI (Fig. 1).

Viral load

The virulence of filoviruses in humans is related to viremia, suggesting that rate of virus replication is an important factor of pathogenesis (Towner et al., 2004). At necropsy, tissue was collected from marmosets for determination of viral load by qRT-PCR. Virus was detected by 3 DPI, resulting in viremia greater than 5 to 7 $\log_{10}$ genome equivalents (GE) per milliliter on the day of necropsy. All tissues contained amounts of viral RNA comparable with levels of viremia (Table 2). At necropsy, differences in peak viral RNA level in the tissues of animals infected with low (10 PFU) and high (1000 PFU) doses of EBOV was observed. Viral load in blood from MARV infected animals ranged from 2.88 $\log_{10}$ at day 2 to 8.15 $\log_{10}$ at day 7.

Gross pathology

Lesions seen in both EBOV marmosets and MARV marmosets were similar. Hepatomegaly was seen in all animals and was often accompanied by multifocal pigmentation and overall discoloration of the liver. Splenomegaly was also a common finding at necropsy. Most animals had lung abnormalities in most lobes, primarily hemorrhage and congestion. Hemorrhage was frequently noted at the site of venipuncture. Other findings included hemorrhage in bladder and adrenals as well as light pigmentation present in lymph nodes.

Histology

Microscopic examination of tissue sections stained with hematoxylin and eosin revealed a number of pathologic lesions (Tables 3 and 4).

Kidney—Renal lesions were observed in all EBOV-infected animals (Fig. 2A), and consisted of fibrin microthrombi lodged within capillary beds of the glomerular tufts. Thrombi were apparent diffusely and often associated with expansion of Bowman's space and accumulation of proteinaceous fluid. Polymorphonuclear cells were infrequently

observed in glomerular tufts and glomerular cells were necrotic. In conjunction, hypoxic nephrosis was evident in the proximal convoluted tubules of most animals and were likely secondary to microthrombosis of the glomerular tufts. MARV-infected animals were dissimilar: renal morphology was within normal limits (Fig. 3A).

Lung—Lungs from all animals revealed fibrin thrombi present within large- to medium-sized pulmonary arteries (Fig. 2B). Thrombi often contained increased numbers of neutrophils and pyknotic debris. Perivascular lymphatics adjacent to these vessels were often dilated and contained protein. Lungs were diffusely congested and multiple foci of fibrin microthrombi were evident in many small arterioles, extending into capillary beds and associated with congestion and hemorrhage. Occasionally extravasated erythrocytes were mixed with evidence of proteinaceous exudates in alveolar spaces.

In contrast, pulmonary changes were minimal to mild in MARV-infected marmosets. One animal (29015) receiving 10 PFU and one receiving 1000 PFU developed mild edema surrounding small pulmonary arteries. In addition, three animals had evidence of a mild focal interstitial pneumonitis characterized by neutrophilic infiltration, septal necrosis and variable alveolar edema. It is unlikely that the pulmonary findings were of clinical significance.

Liver—Hepatic lesions in EBOV-infected marmosets were observed in all animals but differed dependent on the dose and day of death (Fig. 2C). In animals inoculated with 1000 PFU of EBOV, hepatic lesions were mild and consisted of multifocal infiltrates of polymorphonuclear cells within hepatic sinusoids associated with evidence of early necrosis of sinusoidal cells. Viral inclusions were not observed. In animals inoculated with the 10 PFU and surviving to 5 dpi, hepatic disease was more severe and characterized by multifocal to coalescing hepatocellular coagulative necrosis infiltrated by small to moderate numbers of neutrophils. Hepatocytes within and adjacent to these regions of necrosis often contained large amphophilic intracytoplasmic inclusions (Fig. 2D). Inclusions had an asymmetric perinuclear distribution. These more severe changes were accompanied by intracellular biliary stasis. The findings suggest initial targeting of resident sinusoidal cells (Kupffer and monocytes) with subsequent extension to adjacent hepatocytes.

MARV-infected animals all displayed multifocal to coalescing hepatocellular necrosis. Necrotic foci varied from individual hepatocytes to small aggregates of cells up to 300 μm in diameter. Necrotic hepatocytes had rounded and deeply eosinophilic homogeneous to granular appearing cytoplasm with pyknotic or karyorrhectic nuclei (Fig. 3B). Occasionally, hepatocytes in the early phases of degeneration had well defined eosinophilic bodies present within the cytoplasm (eosinophilic degeneration) but the amphophilic inclusions were infrequently observed (Fig. 3C). Dispersed within and adjacent to these regions of necrosis were increased numbers of neutrophils found within sinusoids and mixed with the necrotic debris. In four animals there was evidence of mild to moderate hepatocellular dissociation. The degree of hepatocellular necrosis was similar regardless of inoculum.

Spleen—Spleens of all EBOV-infected animals were depleted of lymphocytes and contained deposits of fibrin (Fig. 2E). Extensive fibrin deposits were observed within the red pulp. These changes were accompanied by necrosis of cells within the Cords of Billroth in severely affected animals. Lymphocyte depletion was severe and appears to be focused on periarteriolar sheaths (T cell regions) and to a lesser extent follicular (B cell) regions. In most residual areas of white pulp, pyknotic and karyorrhectic nuclear debris was evident and these regions were infiltrated by polymorphonuclear cells at multiple foci. In marmosets given 1000 PFU of virus, involvement of B cell regions was significantly less. In contrast, all animals receiving 1000 PFU MARV inoculum had evidence of marked lymphocyte

depletion and lymphoid necrosis in the spleen (Fig. 3D and 3E). Periarteriolar sheaths and follicular B cell areas were reduced in size and contained pyknotic and karyorrhectic debris. The changes were present to a lesser degree in the 10 PFU group, suggesting that viral dose may have been responsible for the observed differences. Fibrin deposition was observed in the medullary cords and correlated with the degree of lymphoid necrosis and lymphocytic depletion.

Lymph node (axillary)—In two EBOV animals, mild to moderate lymphocytic hyperplasia was observed in cortical parafollicular regions, accompanied by increased numbers of tingible body macrophages. In these nodes, scattered areas of hemorrhage and necrosis were occasionally apparent. In contrast, in the two remaining animals, there was evidence of extensive lymphocytic necrosis that was focused in medullary and parafollicular regions, while follicles were spared. These changes were accompanied by hemorrhage, neutrophilic infiltration and extensive fibrin deposition (Fig. 2F).

Changes in lymph node morphology were apparent in only 2 of 6 MARV-infected animals, and consisted of mild to moderate lymphoid necrosis and lymphocytic depletion. In the remaining animals, there was an absence of secondary follicles with germinal centers but lymphocyte numbers appeared normal (Fig. 3F).

Adrenal gland—Fibrin microthrombi were observed in the adrenal glands of some EBOV-infected animals and were most frequently observed in the subcapsular region in the zona glomerulosa. Thrombi were accompanied by congestion and hemorrhage. Multifocal dissociation and necrosis of cortical adrenocytes was evident in a subset of animals and was occasionally accompanied by infiltration by a small number of polymorphonuclear cells. No viral inclusions were evident. Fibrin was not observed in MARV animals. Within adrenal glands there were multiple scattered areas of necrosis of individual and small aggregates of adrenocytes accompanied by the presence of erythrocytes, lymphocytes and mononuclear cells.

Other organs—Lesions were observed inconsistently in other organs and were often related to the effects of disseminated intravascular coagulation and terminal hypoxia. These included evidence of myocardial hypoxic necrosis, and microhemorrhages in the brain, heart, urinary bladder and pancreatic islets. Two animals infected with 1000 PFU of MARV had evidence of a mild focal fibrosis, which dissected along muscle fascicles and was associated with scant histiocytic and lymphocytic infiltrates. Findings in other organs were unremarkable.

Discussion

We report for the first time that the common marmoset is susceptible to experimental infection with viruses from the family *Filoviridae*. The intramuscular inoculation of as little as 10 PFU of either EBOV or MARV induced pathological features similar to those observed in human disease. Most notably, animals experienced thrombocytopenia, neutrophilia and disseminated intravascular coagulation. Furthermore, the small nonhuman primate experiences a disease syndrome comparable to what has been reported in other nonhuman primate models currently used to study filovirus disease.

Cynomolgus macaques are frequently used in preclinical testing of filovirus vaccine and therapeutic strategies and are considered the "gold standard" animal model (Bente et al., 2009). Experimental EBOV infection of macaques by intramuscular injection of 1000 PFU of virus results in a rapid fatal disease [30,36]. Beginning at 4 DPI, macaques experienced anorexia coinciding with the onset of fever. Shortly after these initial findings, petechial rash

was seen with varying degrees of recumbency, culminating in prostration and death at 7 days post-challenge (Geisbert et al., 2003d). We observed a similar, although shortened (death 4-5 DPI), course of disease in marmosets infected with EBOV. Previous work has shown that intramuscular inoculation of macaques with MARV results in an analogous course of disease; however, overall disease progression was delayed with death occurring between days 8 and 13 (Bente et al., 2009; Geisbert et al., 2007; Jaax et al., 1996). Consistent with the macaque model, experimental inoculation of marmosets with MARV also results in delayed onset of disease, with death occurring 3 to 4 days later than that seen with marmosets infected with EBOV. However, the course of Marburg disease in marmosets was more rapid than that seen in macaques, with death occurring at 6 to 8 DPI. Although not statistically significant, it is interesting to note that MARV infected marmosets had an average time to death 1 day shorter than those receiving a high dose of virus.

Human filovirus infection is marked by neutrophilia, lymphopenia and thrombocytopenia. These findings are observed in the macaque model of filovirus disease and are used as surrogate markers of disease progression for *in vivo* studies (Geisbert et al., 2003b; Simpson, 1969; Simpson et al., 1968). Marmosets infected with either of the filoviruses also display these hematological abnormalities. Beginning at 2 DPI, overall platelet counts decreased while neutrophil numbers increased, with a concomitant decrease in lymphocyte numbers (Fig. 1).

Autopsy findings from fatal human cases reveal hepatomegaly with necrotic foci observed throughout liver. Likewise, experimentally infected macaques developed numerous hepatic lesions (Geisbert et al., 2008; Geisbert et al., 2003b; Geisbert et al., 2003c; Geisbert et al., 2003d; Jaax et al., 1996). The marmoset showed biochemical signs of liver involvement early in infection: markers of liver function (ALT, ALP, GGT) reached levels in excess of 30-fold above baseline at necropsy. Consistent with high-levels of liver enzymes, gross examination of the liver revealed hepatomegaly with pale foci throughout all lobes. Microscopic examination of sections from the liver revealed necrosis with mild to moderate inflammation. Hepatic changes did not appear to be virus dose-dependent, although further animal or morphometric studies would be needed to confirm this. Evidence of mild to moderate hepatocellular fatty change was present. Similar findings have been documented in the macaque model of filovirus infection and most importantly, the findings reported here are comparable to those reported in fatal human cases (Geisbert et al., 2008; Geisbert et al., 2003b; Geisbert et al., 2003c; Jaax et al., 1996).

One difference between the macaque model of filovirus infection and marmosets is that marmosets do not develop a petechial rash. In this respect, they appear to be more similar to the African green monkey model of filovirus infection (Bente et al., 2009; Davis et al., 1997). We speculate that the rapid disease progression preempts its development. Nonetheless, clear signs of coagulation abnormalities are pronounced, as animals experience thrombocytopenia, hemorrhage and bleeding at sites of venipuncture. Fatal human cases are characterized by hemorrhage and bleeding at site of venipuncture and other coagulation abnormalities. The coagulopathy observed in humans at times exists in the absence of rash: only 50% of patients infected with EBOV develop a maculopapular rash (Bwaka et al., 1999). Further evidence that the marmoset mimics human disease is that microscopic examination of tissue from EBOV-infected animals reveals widespread fibrin deposition that is a hallmark of coagulation abnormalities (Geisbert et al., 2003c; Geisbert et al., 2003d; Jaax et al., 1996). EBOV infection of the marmoset caused a severe disseminated viral infection characterized principally by microthrombosis in multiple organs (disseminated intravasculature coagulation). To a lesser degree, MARV-infected animals displayed moderate fibrin deposition in the spleen. A similar observation has been reported for rhesus macaques infected with *Marburgvirus* Angola where deposition of polymerized fibrin was

less pronounced than in EBOV infected macaques (Geisbert et al., 2007). These findings are similar to that seen in human infection and the macaque (Geisbert et al., 2003a; Geisbert et al., 2003b; Geisbert et al., 2003c; Jaax et al., 1996). Signs of coagulopathy characteristic of primate infections are observed variably in rodent models (Bente et al., 2009; Bray et al., 1999; Connolly et al., 1999).

High levels of viremia in human filovirus infections are associated with high mortality. A 2-log difference in titers is sufficient to predict clinical outcomes (Towner et al., 2004). Inoculation of macaques with either EBOV or MARV results in high viral loads in both blood and tissue (Geisbert et al., 2003d). In the current study, all marmosets had high virus loads ($>10^6$) in blood and tissue regardless of dose or agent. Consistent with human cases, virus was widely disseminated, with the spleen and liver frequently having levels 1-log higher than other tissue. In animals given 1000 PFU EBOV, viral load was 2-logs less than those in animals receiving 10 PFU of virus. This difference could be a result of a rapid onset of morbidity affecting viral load. Virus load in animals infected with MARV was similar and likely the result of relatively longer time to death compared to EBOV animals. It is worthwhile noting that recently it has been shown that filovirus replication results in a surplus of genomes with varying degrees of packaging efficiency and infectious particles. In the in vitro studies, the ratio of RNA to focus forming units was 100-fold more in EBOV versus MARV (Weidmann et al., 2011). Taking this into account, the difference in virus load between MARV and EBOV infected marmosets may be correspondingly different.

Differences in histopathology were observed between animals inoculated with MARV and EBOV. EBOV infection resulted in widespread intravascular coagulation apparent in multiple organs including the spleen, adrenal gland, kidney and lung (Fig. 2 and Table 3). There was evidence of extensive lymphocytic necrosis focused in medullary and parafollicular regions, while follicles were spared. These changes were accompanied by hemorrhage, neutrophilic infiltration and extensive fibrin deposition (Fig. 2F). Findings suggest initial activation within T lymphocyte areas followed by subsequent and rapid lymphocytic depletion, most likely through apoptotic mechanisms. Comparing changes to changes observed in the spleen suggests alterations in the lymph node lag behind those observed in the spleen. MARV animals inoculated with 1000 PFU had moderate fibrin deposition in the spleen, widespread intravascular coagulation was not observed, suggesting a significant difference in pathogenesis between the two agents (Fig. 3 and Table 4).

The observation that hepatic lesions are less severe in animals receiving high dose of virus versus a lower dose is difficult to explain with a small sample size. The virus preparation used to infect the monkeys was prepared at a low moi in order to minimize the effect of DI particles. It is known in filovirus infection, hepatic lesions early in infection are less severe than those at terminal endpoints (Geisbert 2003). Perhaps the relatively quick time to death in those animals infected with high dose of virus preempted the development of severe liver pathology.

Our study has shown that intramuscular inoculation of marmosets with EBOV or MARV causes hemorrhagic fever reminiscent of human infection. Since nonhuman primates are more predictive of filovirus therapeutic efficacy than rodents, the small-sized marmoset is a viable alternative small animal model. The marmoset size is comparable to that of a guinea pig, making it attractive for testing therapeutic reagents that are only available in small quantities. In addition, the neotropical monkey can serve to alleviate the shortage of macaques available for research (Patterson and Carrion, 2005; Satkoski et al., 2008). That the common marmoset is susceptible to wild-type, non-adapted virus is especially attractive to those wishing to evaluate countermeasures in a small animal model with viruses derived from fatal human cases.

Materials and Methods

Biosafety

EBOZ and *MARV* are Risk Group 4, Category A biothreat agents. All experiments with this virus were performed within a biosafety level 4 (BSL4) facility by personnel in a biosafety suit at the Texas Biomedical Research Institute (San Antonio, TX). Both the Institutional Animal Care and Use Committee and the Institutional Biohazards Committee at Texas Biomed approved experimental protocols.

Virus strains

EBOV (Kikwit) and *MARV* Musoke were provided by Dr. Peter Jahrling (USAMRIID, Fort Detrick, Maryland). Stocks were used to infect tissue culture flasks containing Vero E6 cells at 90% confluency. The flasks were infected at an MOI of 0.01 then incubated until cytopathic effect greater than 80% was observed then harvested and stored in aliquots in an ultralow temperature freezer. Infectivity of virus stocks was determined by plaque titration (Moe et al., 1981).

Animals

Ten adult marmosets ranging in weight from 331 g to 425 g were obtained from the Southwest National Primate Research Center in San Antonio, Texas. One week before the start of the study, animals were transferred to the BSL4 facility at Texas Biomed and housed individually in a climate controlled caging. At day 0, animals were injected intramuscularly (0.5 mL) with either EBOV (10 PFU, *n*=2; 1000 PFU, *n*=2) or MARV (10 PFU, *n*=2; 1000 PFU, *n*=4) diluted in PBS. Animals were sedated and blood was collected at day 0, 2, 5 and 7 for analysis. Animals were euthanized when moribund using approved methods. All procedures were approved by the Texas Biomed Institutional Animal Care and Use Committee and were performed in accordance with applicable federal guidelines.

Hematology and blood chemistry

Biochemical analysis of plasma samples was performed using mammalian liver enzyme profile rotor on Vet Scan analyzer (Abaxis, Inc., Union City, CA). Complete blood counts were performed using a Vet HMT machine (Abaxis, Inc., Union City, CA).

Tissue preparation and staining

Tissue was collected using sterilized scalpels and forceps. To minimize contamination of tissue with blood, tissue samples were harvested after blood collection. Aseptically collected tissues were fixed in phosphate-buffered 4% paraformaldehyde (pH 7.2) and embedded in paraffin for histological examination. Paraffin-embedded tissues were cut in 5-μm sections, deparaffinized and stained with hematoxylin and eosin.

Total RNA isolation and qRT-PCR

Viral load in tissues were measured by quantitative RT-PCR (qRT-PCR). Tissue was homogenized with Trizol Reagent (Invitrogen) using the TissueLyser (Qiagen Inc., Valencia, CA) homogenization system and RNA extracted per the manufacturer's recommendations. Real-time qRT-PCR was performed using an ABI PRISM 7700 Sequence Detection System (Applied Biosystems, Foster City, CA) and RNA Ultrasense one-step real-time qRT-PCR system (Invitrogen). The EBOV qRT-PCR assays were performed as previously described (Sun et al., 2009). MARV qRT-PCR was performed as described above using a primer/probe set directed at a region within the MARV glycoprotein (MAGP-F: 5′GGCCTTCAGGGCAGGTGTA 3′, MAGP-R : 5′ CCTGTGCATGAGGGTTTTGA 3′, MMGP-Probe: 5′ FAM-CCTTGCTGTTAGATCCTCCTACCAA-TAMRA 3′).

Acknowledgments

References

Adams AP, Aronson JF, Tardif SD, Patterson JL, Brasky KM, Geiger R, de la Garza M, Carrion R Jr, Weaver SC. Common marmosets (Callithrix jacchus) as a nonhuman primate model to assess the virulence of eastern equine encephalitis virus strains. J Virol. 2008; 82:9035–9042. [PubMed: 18614636]

Avila MM, Frigerio MJ, Weber EL, Rondinone S, Samoilovich SR, Laguens RP, de Guerrero LB, Weissenbacher MC. Attenuated Junin virus infection in Callithrix jacchus. J Med Virol. 1985; 15:93–100. [PubMed: 2981980]

Avila MM, Samoilovich SR, Laguens RP, Merani MS, Weissenbacher MC. Protection of Junin virus-infected marmosets by passive administration of immune serum: association with late neurologic signs. J Med Virol. 1987; 21:67–74. [PubMed: 3025358]

Bente D, Gren J, Strong JE, Feldmann H. Disease modeling for Ebola and Marburg viruses. Dis Model Mech. 2009; 2:12–17. [PubMed: 19132113]

Bray M, Davis K, Geisbert T, Schmaljohn C, Huggins J. A mouse model for evaluation of prophylaxis and therapy of Ebola hemorrhagic fever. J Infect Dis. 1999; 179(Suppl 1):S248–258. [PubMed: 9988191]

Bright H, Carroll AR, Watts PA, Fenton RJ. Development of a GB virus B marmoset model and its validation with a novel series of hepatitis C virus NS3 protease inhibitors. J Virol. 2004; 78:2062–2071. [PubMed: 14747571]

Bwaka MA, Bonnet MJ, Calain P, Colebunders R, De Roo A, Guimard Y, Katwiki KR, Kibadi K, Kipasa MA, Kuvula KJ, Mapanda BB, Massamba M, Mupapa KD, Muyembe-Tamfum JJ, Ndaberey E, Peters CJ, Rollin PE, Van den Enden E. Ebola hemorrhagic fever in Kikwit, Democratic Republic of the Congo: clinical observations in 103 patients. J Infect Dis. 1999; 179(Suppl 1):S1–7. [PubMed: 9988155]

Carrion R Jr, Brasky K, Mansfield K, Johnson C, Gonzales M, Ticer A, Lukashevich I, Tardif S, Patterson J. Lassa virus infection in experimentally infected marmosets: liver pathology and immunophenotypic alterations in target tissues. J Virol. 2007a; 81:6482–6490. [PubMed: 17409137]

Carrion R Jr, Patterson JL, Johnson C, Gonzales M, Moreira CR, Ticer A, Brasky K, Hubbard GB, Moshkoff D, Zapata J, Salvato MS, Lukashevich IS. A ML29 reassortant virus protects guinea pigs against a distantly related Nigerian strain of Lassa virus and can provide sterilizing immunity. Vaccine. 2007b; 25:4093–4102. [PubMed: 17360080]

Connolly BM, Steele KE, Davis KJ, Geisbert TW, Kell WM, Jaax NK, Jahrling PB. Pathogenesis of experimental Ebola virus infection in guinea pigs. J Infect Dis. 1999; 179(Suppl 1):S203–217. [PubMed: 9988186]

Davis KJ, Anderson AO, Geisbert TW, Steele KE, Geisbert JB, Vogel P, Connolly BM, Huggins JW, Jahrling PB, Jaax NK. Pathology of experimental Ebola virus infection in African green monkeys. Involvement of fibroblastic reticular cells. Arch Pathol Lab Med. 1997; 121:805–819. [PubMed: 9278608]

Feldmann H, Jones S, Klenk HD, Schnittler HJ. Ebola virus: from discovery to vaccine. Nat Rev Immunol. 2003; 3:677–685. [PubMed: 12974482]

Geisbert TW, Daddario-DiCaprio KM, Geisbert JB, Young HA, Formenty P, Fritz EA, Larsen T, Hensley LE. Marburg virus Angola infection of rhesus macaques: pathogenesis and treatment with recombinant nematode anticoagulant protein c2. J Infect Dis. 2007; 196(Suppl 2):S372–381. [PubMed: 17940973]

Geisbert TW, Daddario-DiCaprio KM, Williams KJ, Geisbert JB, Leung A, Feldmann F, Hensley LE, Feldmann H, Jones SM. Recombinant vesicular stomatitis virus vector mediates postexposure protection against Sudan Ebola hemorrhagic fever in nonhuman primates. J Virol. 2008; 82:5664–5668. [PubMed: 18385248]

Geisbert TW, Hensley LE, Jahrling PB, Larsen T, Geisbert JB, Paragas J, Young HA, Fredeking TM, Rote WE, Vlasuk GP. Treatment of Ebola virus infection with a recombinant inhibitor of factor VIIa/tissue factor: a study in rhesus monkeys. Lancet. 2003a; 362:1953–1958. [PubMed: 14683653]

Geisbert TW, Hensley LE, Larsen T, Young HA, Reed DS, Geisbert JB, Scott DP, Kagan E, Jahrling PB, Davis KJ. Pathogenesis of Ebola hemorrhagic fever in cynomolgus macaques: evidence that dendritic cells are early and sustained targets of infection. Am J Pathol. 2003b; 163:2347–2370. [PubMed: 14633608]

Geisbert TW, Pushko P, Anderson K, Smith J, Davis KJ, Jahrling PB. Evaluation in nonhuman primates of vaccines against Ebola virus. Emerg Infect Dis. 2002; 8:503–507. [PubMed: 11996686]

Geisbert TW, Young HA, Jahrling PB, Davis KJ, Kagan E, Hensley LE. Mechanisms underlying coagulation abnormalities in ebola hemorrhagic fever: overexpression of tissue factor in primate monocytes/macrophages is a key event. J Infect Dis. 2003c; 188:1618–1629. [PubMed: 14639531]

Geisbert TW, Young HA, Jahrling PB, Davis KJ, Larsen T, Kagan E, Hensley LE. Pathogenesis of Ebola hemorrhagic fever in primate models: evidence that hemorrhage is not a direct effect of virus-induced cytolysis of endothelial cells. Am J Pathol. 2003d; 163:2371–2382. [PubMed: 14633609]

Greenough TC, Carville A, Coderre J, Somasundaran M, Sullivan JL, Luzuriaga K, Mansfield K. Pneumonitis and multi-organ system disease in common marmosets (Callithrix jacchus) infected with the severe acute respiratory syndrome-associated coronavirus. Am J Pathol. 2005; 167:455–463. [PubMed: 16049331]

Groseth A, Feldmann H, Strong JE. The ecology of Ebola virus. Trends Microbiol. 2007; 15:408–416. [PubMed: 17698361]

Jaax NK, Davis KJ, Geisbert TJ, Vogel P, Jaax GP, Topper M, Jahrling PB. Lethal experimental infection of rhesus monkeys with Ebola-Zaire (Mayinga) virus by the oral and conjunctival route of exposure. Arch Pathol Lab Med. 1996; 120:140–155. [PubMed: 8712894]

Jacob JR, Lin KC, Tennant BC, Mansfield KG. GB virus B infection of the common marmoset (Callithrix jacchus) and associated liver pathology. J Gen Virol. 2004; 85:2525–2533. [PubMed: 15302946]

Jahrling PB, Geisbert J, Swearengen JR, Jaax GP, Lewis T, Huggins JW, Schmidt JJ, LeDuc JW, Peters CJ. Passive immunization of Ebola virus-infected cynomolgus monkeys with immunoglobulin from hyperimmune horses. Arch Virol Suppl. 1996; 11:135–140. [PubMed: 8800795]

Lukashevich IS, Carrion R Jr, Salvato MS, Mansfield K, Brasky K, Zapata J, Cairo C, Goicochea M, Hoosien GE, Ticer A, Bryant J, Davis H, Hammamieh R, Mayda M, Jett M, Patterson J. Safety, immunogenicity, and efficacy of the ML29 reassortant vaccine for Lassa fever in small non-human primates. Vaccine. 2008; 26:5246–5254. [PubMed: 18692539]

Mansfield K. Marmoset models commonly used in biomedical research. Comp Med. 2003; 53:383–392. [PubMed: 14524414]

Moe JB, Lambert RD, Lupton HW. Plaque assay for Ebola virus. J Clin Microbiol. 1981; 13:791–793. [PubMed: 7014628]

Patterson JL, Carrion R Jr. Demand for nonhuman primate resources in the age of biodefense. ILAR J. 2005; 46:15–22. [PubMed: 15644560]

Peterson AT, Bauer JT, Mills JN. Ecologic and geographic distribution of filovirus disease. Emerg Infect Dis. 2004a; 10:40–47. [PubMed: 15078595]

Peterson AT, Carroll DS, Mills JN, Johnson KM. Potential mammalian filovirus reservoirs. Emerg Infect Dis. 2004b; 10:2073–2081. [PubMed: 15663841]

Samoilovich SR, Pecci Saavedra J, Frigerio MJ, Weissenbacher MC. Nasal and intrathalamic inoculations of primates with Tacaribe virus: protection against Argentine hemorrhagic fever and absence of neurovirulence. Acta Virol. 1984; 28:277–281. [PubMed: 6148851]

Satkoski JA, Malhi R, Kanthaswamy S, Tito R, Malladi V, Smith D. Pyrosequencing as a method for SNP identification in the rhesus macaque (Macaca mulatta). BMC Genomics. 2008; 9:256. [PubMed: 18510772]

Simpson DI. Marburg agent disease: in monkeys. Trans R Soc Trop Med Hyg. 1969; 63:303–309. [PubMed: 4978540]

Simpson DI, Zlotnik I, Rutter DA. Vervet monkey disease. Experiment infection of guinea pigs and monkeys with the causative agent. Br J Exp Pathol. 1968; 49:458–464. [PubMed: 5727750]

Sun Y, Carrion R Jr, Ye L, Wen Z, Ro YT, Brasky K, Ticer AE, Schwegler EE, Patterson JL, Compans RW, Yang C. Protection against lethal challenge by Ebola virus-like particles produced in insect cells. Virology. 2009; 383:12–21. [PubMed: 18986663]

Towner JS, Rollin PE, Bausch DG, Sanchez A, Crary SM, Vincent M, Lee WF, Spiropoulou CF, Ksiazek TG, Lukwiya M, Kaducu F, Downing R, Nichol ST. Rapid diagnosis of Ebola hemorrhagic fever by reverse transcription-PCR in an outbreak setting and assessment of patient viral load as a predictor of outcome. J Virol. 2004; 78:4330–4341. [PubMed: 15047846]

Weatherford T, Chavez D, Brasky KM, Lanford RE. The marmoset model of GB virus B infections: adaptation to host phenotypic variation. J Virol. 2009; 83:5806–5814. [PubMed: 19279089]

Weidmann M, Sall AA, Manuguerra JC, Koivogui L, Adjami A, Traore FF, Hedlund KO, Lindegren G, Mirazimi A. Quantitative analysis of particles, genomes and infectious particles in supernatants of haemorrhagic fever virus cell cultures. Virol J. 2011; 8:81. [PubMed: 21349180]

Weissenbacher MC, Avila MM, Calello MA, Merani MS, McCormick JB, Rodriguez M. Effect of ribavirin and immune serum on Junin virus-infected primates. Med Microbiol Immunol. 1986a; 175:183–186. [PubMed: 3014292]

Weissenbacher MC, Calello MA, Merani MS, McCormick JB, Rodriguez M. Therapeutic effect of the antiviral agent ribavirin in Junin virus infection of primates. J Med Virol. 1986b; 20:261–267. [PubMed: 3023541]

Weissenbacher MC, Coto CE, Calello MA, Rondinone SN, Damonte EB, Frigerio MJ. Cross-protection in nonhuman primates against Argentine hemorrhagic fever. Infect Immun. 1982; 35:425–430. [PubMed: 6276301]

Zampieri CA, Sullivan NJ, Nabel GJ. Immunopathology of highly virulent pathogens: insights from Ebola virus. Nat Immunol. 2007; 8:1159–1164. [PubMed: 17952040]
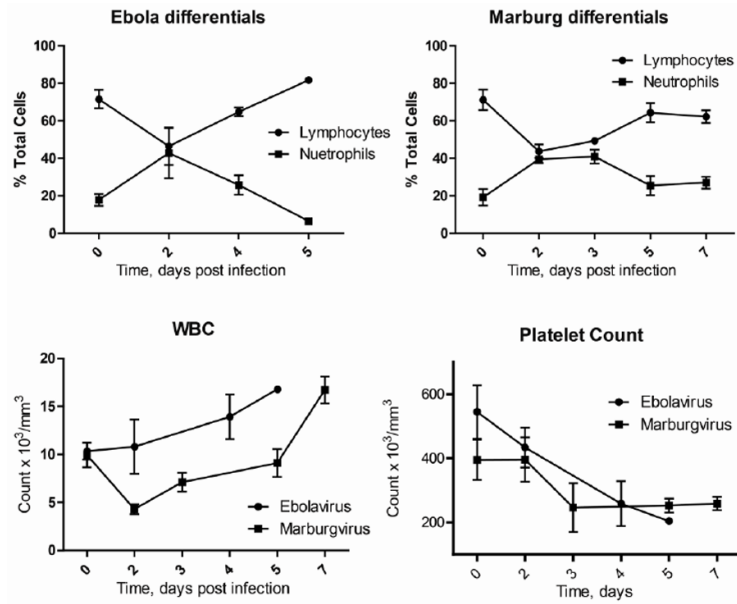
Fig. 1.
Hematology data from marmosets experimentally inoculated with filoviruses. Animals infected with both *Ebolavirus* (top left) and *Marburgvirus* (top right) developed neutrophilia with a concomitant decrease in lymphocytes. Total white blood counts (bottom left) increased during the course of infection while thrombocytopenia (bottom right) developed. Because of the limited samples size, data points are represented as geometrical means of data corresponding to timepoint regardless of virus dose.
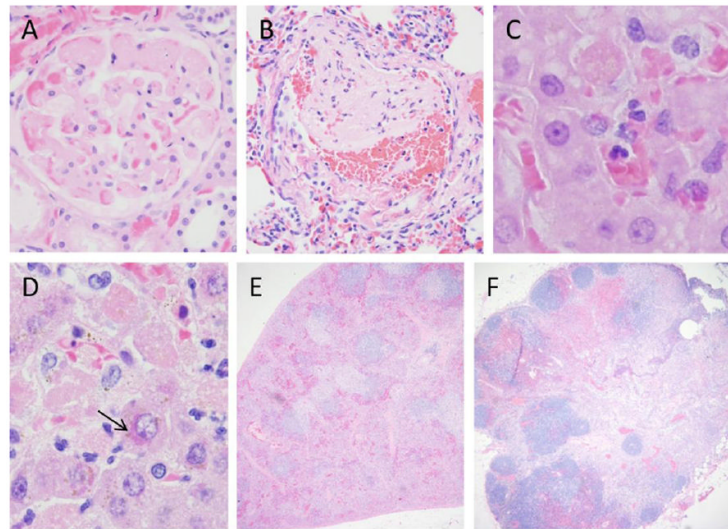
Fig. 2.
Pathology of EBOV viral infection in common marmosets. Inoculation of EBOV virus produced disseminated microvascular thrombosis evident in glomerular capillaries (A) and lung (B). Multifocal focal hepatic necrosis (C) and characteristic intracytoplasmic viral inclusions were evident (D, arrow). Lymphoid necrosis was observed in the spleen (E) and peripheral lymph nodes (F). Fibrin deposition was widespread in medullary cords of the spleen (E).
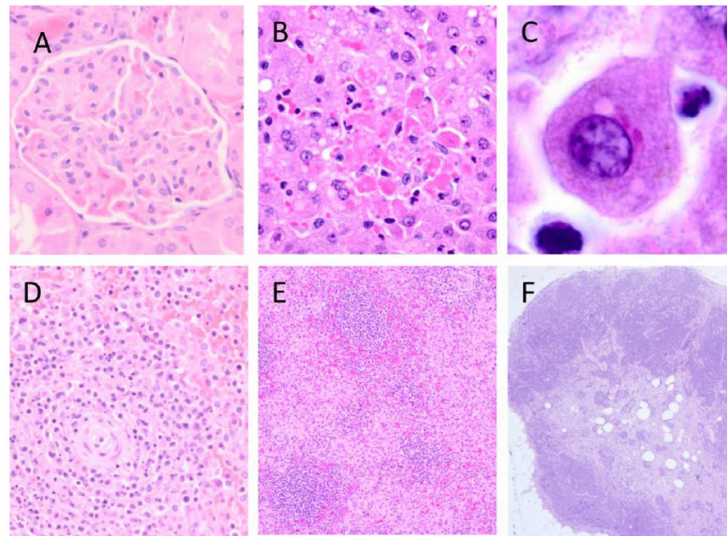
Fig. 3.
Pathology of MARV virus infection in common marmosets. Microvascular glomerular thrombosis was not observed in animals inoculated with MARV virus and glomeruli (A) appeared histologically normal. Multifocal hepatic necrosis (B) and characteristic intracytoplasmic hepatocellular viral inclusions were observed (C). Lymphoid necrosis within periarteriolar sheaths of the spleen (D) and fibrin deposition within splenic medullary cords (E) was evident. In contrast to EBOV infection peripheral lymph nodes appeared normal (F).

Table 1

Clinical chemistry from filovirus infected marmosets.

Animal number	Inoculumn	Dose (PFU)	ALP[a]	ALT[a]	GGT[a]
28707	EBOV	10	21	362	94
28709	EBOV	1000	83	22	<5
28705	EBOV	1000	49	10	6
28716	EBOV	10	>2400	1341	578
29003	MARV	1000	1350	349	1440
29005	MARV	1000	355	463	2049
28554	MARV	1000	1069	406	1985
29784	MARV	1000	1101	606	>3000
29015	MARV	10	639	714	429
29018	MARV	10	319	381	1394

[a]Peak value after experimental infection noted in U/L

Table 2

Viral load in filovirus infected marmoset tissue.

Tissue	Log$_{10}$ genome equivalents/100 mg tissue[a]			
	Ebola (10 pfu)	Ebola (10^3 pfu)	Marburg (10 pfu)	Marburg (10^3 pfu)
Adrenal	8.348	7.493	7.899	7.98
Bladder	7.387	6.051	6.827	7.498
Brain	5.761	5.179	6.965	6.968
Colon	6.6	5.093	6.835	7.089
Duodenum	7.609	5.758	5.702	7.481
Heart	6.322	5.364	7.856	7.573
Ileum	6.614	5.525	6.276	6.97
Kidney	7.916	6.532	7.448	7.604
Liver	7.715	6.364	8.178	8.277
Lung	5.966	6.749	8.003	7.898
Lymph nodes	8.152	7.245	7.171	7.25
Muscle	6.584	6.045	7.966	7.116
Pancreas	6.186	4.842	6.574	6.974
Spleen	6.983	7.587	8.051	8.561
Stomach	6.963	5.121	5.42	6.779

[a] Viral load is represented as geometric mean of two animals per group.

Table 3

Histologic findings in marmosets inoculated with EBOV.

Animal number	28709	28705	28707	28716
Dose	10^3 pfu	10^3 pfu	10 pfu	10 pfu
Survival (days)	4	4	5	5
Liver				
Necrosis	+	+	++	+++
Inclusion	–	–	present	present
Adrenal				
Thrombi	++	–	++	–
Necrosis	++	–	++	+
Lung				
Thrombi	++	+	++	+
Hemorrhage and congestion	++	+	++	+
Spleen				
Lymphoid depletion	+	+	++	+++
Fibrin deposition	++	++	++	+++
Lymph node				
Lymphoid hyperplasia	–	++	–	++
Lymphoid depletion	+++	+	+++	+
Neutrophilic infiltrates	++	+	+	+
Hemorrhage	++	+	+++	+
Urinary tract				
Glomerular tufts fibrin	++	+++	++	++
Hypoxic nephrosis	++	+++	++	+
Hemorrhage bladder	+	++	n/a	–

– is absence of lesion;

+ is mildly;

++ moderately affected;

+++ severely affected

Table 4

Histologic findings in MARV virus inoculated animals.

Animal number	29003	29005	28554	29784	29015	29018
Dose	10³ pfu	10³ pfu	10³ pfu	10³ pfu	10 pfu	10 pfu
Survival (days)	**8**	**7**	**8**	**7**	**6**	**7**
Liver						
Hepatic necrosis	++	++	++	++	++	++
Hepatocellular dissociation	++	−	+	+	−	+
Neutrophilic infiltrates	+	+	+	+	+	+
Hepatocellular fatty change	++	−	+	+	+	−
Adrenal						
Extramedullary hematopoiesis	−	−	+	++	−	+
Adrenalitis/necrosis	+	+	+	+	++	+
Lung						
Pneumonitis	−	−	+	+	+	−
Perioarteriolar edema	+	−	−	−	+	−
Spleen						
Necrosis	++++	+++	+++	++++	+	++
Lymphocytic depletion	+++	+++	+++	++++	+	++
Fibrin deposition medullary cords	++	++	++	++	+	+
Lymph node						
Necrosis	++	−	n/a	+	−	−
Lymphocytic depletion	+	−	+	+	−	−
Thymus	−	n/a	+	n/a	−	n/a
Bone marrow, kidney, heart, skeletal muscle, brain, gastrointestinal tissue	PMA	WNL	WNL	WNL	WNL	WNL

− is absence of lesion;

+ is mildly affected;

++ moderately affected;

+++ severely affected

WNL is within Normal Limits